Design of a morphing actuated aileron
with chiral composite internal structure

Alessandro Airoldi[*], Giuseppe Quaranta, Alvise Beltramin and Giuseppe Sala

*Department of Aerospace Science and Technology, Politecnico di Milano,
Via La Masa 34, 20156, MILANO, ITALY*

Abstract. The paper presents the development of numerical models referred to a morphing actuated aileron. The structural solution adopted consists of an internal part made of a composite chiral honeycomb that bears a flexible skin with an adequate combination of flexural stiffness and in-plane compliance. The identification of such structural frame makes possible an investigation of different actuation concepts based on diffused and discrete actuators installed in the skin or in the skin-core connection. An efficient approach is presented for the development of aeroelastic condensed models of the aileron, which are used in sensitivity studies and optimization processes. The aerodynamic performances and the energy required to actuate the morphing surface are evaluated and the definition of a general energetic performance index makes also possible a comparison with a rigid aileron. The results show that the morphing system can exploit the fluid-structure interaction in order to reduce the actuation energy and to attain considerable variations in the lift coefficient of the airfoil.

Keywords: smart structures; chiral topologies; morphing structures; aeroelastic design

1. Introduction

The aerodynamic forces acting on an aircraft depend on the external shape of the aerodynamic surfaces. Therefore, shape variation is a typical characteristic of aeronautical structures and it is used for the generation of forces required to control the aircraft, and for the optimization of the aerodynamic performances during different mission segments.

In recent years, researchers have carried out considerable efforts to conceive and develop flexible structures capable of smooth and progressive external shape changing, which are typically referred to as morphing structures. Although different definitions of morphing structures exist, the distinctive aspects of morphing system is the possibility of continuous shape variations that can be seen as an alternative to the rigid motion of moveable surfaces, such as flaps or ailerons, driven by internal mechanisms.

Actually, flexible structures for guidance, control and adaptation to flight conditions were taken into account since the beginning of human flight, as it is proved by the solution devised in the Wright's flyer to attain control around the roll axis (see Anderson 1999). However, the increasing flight speeds and the consequent higher structural loads rapidly lead to discard such solutions in

---

*Corresponding author, Assistant Professor, E-mail: alessandro.airoldi@polimi.it

favor of more rigid and robust systems, such as the control surfaces that can be found in modern conventional aircraft.

The renewed interest in morphing surfaces has been driven by several factors, such as the search for an enhanced operative flexibility of aircrafts, the increasing demand for low fuel consumptions and, consequently, the requirements for optimal shapes in different mission segments, and the design of unmanned aerial vehicles (UAV), which represent an interesting benchmark for the development of innovative technologies. Moreover, the technological advancement in the area of new materials and of distributed actuation systems represents a fundamental driving factor for morphing systems, since they suggest unforeseen possibilities and are fundamental to devise efficient and lightweight systems.

Recent reviews, such as Barbarino *et al.* (2013) and Sofla *et al.* (2010), have presented a large number of morphing solutions, which have been classified according to the type of shape variation they are designed to accomplish, such as airfoil camber and thickness changing, planform alteration and out-of-plane transformation. From the structural point of view, all the solutions are characterized by different choices regarding three basic aspects of the system, namely the internal structure, the external flexible skin and the type of actuation. It can also be observed that some solutions are actually passive morphing systems, which do not require actuation but adapt their shape to the external aerodynamic conditions, such as the wings proposed by Bornengo *et al.* (2005) and Airoldi *et al.* (2012).

In a morphing surface, the internal structure and the skin must be able to change their shapes but also to exhibit adequate load carrying capability and strength. Moreover, the forces and the energy required to achieve shape changing should be minimized, in order to reduce the demand for the actuation system. Therefore, compliance have to be maximized in the direction of shape change, but the system should be able to carry loads in other directions. Shape change must be achieved and maintained against external forces, which are typically represented by aerodynamic loads, and this require actuators having load bearing capability. Such set of requirements is fulfilled in various ways by solutions presented in literature.

The design of a morphing system is a complex task, which can be realistically carried out after the definition of the type morphing structure to be considered. Some interesting examples of design processes can be found in literature considering variable camber airfoils. In the passive solution presented by Airoldi *et al.* (2012a) the design problem is set up by varying the topology and the mechanical properties of the internal structure of the flexible skin. An optimization process is carried out by using a complete aeroelastic model. In active structures, the number and the position of actuators can be optimized, as it presented in the structure idealized by Baker and Friswell (2009) where the position of actuators is chosen in order to minimize the strain required for morphing a variable camber profile. The importance of the aeroelastic interactions is pointed out by Campanile and Anders (2005), considering the belt rib concept originally proposed by Campanile and Sachau (2000). The analytical model developed in Campanile and Anders (2007) shows how aeroelastic interactions can be exploited in order to minimize the work required by actuators.

This paper presents a structural solution for a variable camber airfoil and apply a numerical approach for the design of an active morphing aileron. The internal structure of the aileron is represented by ribs made of chiral composite honeycomb, a well-suited structural topology for morphing applications. Indeed, chiral geometries are non-centrosymmetric topologies which have been originally studied for their peculiar response, characterized by negative Poisson's coefficient, as presented in Lakes (1991). They have been already proposed and assessed for the development

of variable camber airfoils by Bornengo *et al.* (2005), Spadoni and Ruzzene (2007), Martin *et al.*(2008). Moreover, the solution considered in this work takes into account the availability of a technological process for the production of composite chiral structures, which has been developed and assessed for the productions of chiral units and ribs in Bettini *et al.* (2010) and Airoldi *et al.* (2012b). For the skin, a solution based on a composite corrugate laminate is taken into consideration, which was proposed by Yokozeki *et al.* (2006). The constructive solution is applied to define the structure of the morphing aileron and actuation is introduced considering two different choices, based on a diffused actuation system applied to the skin and on a set of micromotors installed at the connection between the internal structure and the external skin, respectively.

The objective of the paper is to explore the potential performances of these morphing solutions and assessing an effective numerical approach for design purposes, developed by defining a condensed aeroelastic model and suitable to be adopted in sensitivity studies and optimization procedures.

In the following second section of the paper, the structure and the structural model of the aileron will be presented, including the solutions considered for the actuation system and the corresponding idealization to be adopted in simplified models. In the third section, a numerical approach based on a condensed structural model and an aerodynamic panel method is developed and the aeroelastic model is assembled. The application of the model and the results obtained by means of sensitivity studies and optimization processes are described in the fourth section of the paper. Finally, the main findings of the activity are discussed in conclusive remarks.

2. Configuration and numerical idealization of the morphing surface

2.1 Chiral topologies for internal structures of morphing components

The structural configuration of the morphing aileron considered in this work is based on flexible ribs that bear an external morphing cover. A cellular structure is chosen to design a rib capable to fulfill its typical structural functions and to make possible a continuous, smooth shape change without localized deformations.

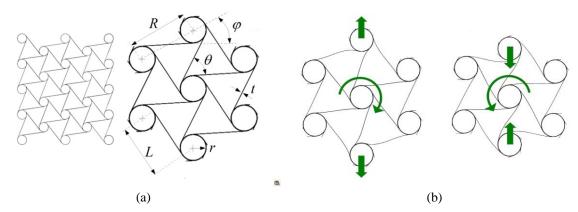(a)   (b)

Fig. 1 (a) Hexa-chiral topology and (b) Deformation mechanism

To meet such conflicting requirements, rib design is based on a chiral topology, which is a non-centro-sysmmetric tessellation that consists of circular elements, called nodes, connected by straight ligaments. The example presented in Fig. 1(a) is referred to hexa-chiral topology, with six ligaments departing from each node. The geometry is characterized by a set of parameters: the distance between the node centers, R, the radius of the node, r, the ligament length, L, the angle φ and the wall thickness, t, whereas angle ϑ is fixed to 30° for the hexa-chiral type. Indeed, application of geometric relations leads to only 3 independent parameters.

The ligaments are tangential to the nodes and tend to wind or unwind about the nodes under the action of a compressive or tensile in-plane force, as it is shown in Fig. 1(b). Such deformation mechanism originates a negative Poisson's ratio (auxetic behavior) up to the theoretical limit of -1 evaluated by Lakes (1991). It is worth noting that a negative Poisson's ratio also involves an inherent stiffness to local shape changing, because, considering the topology as a meta-material, it increases the shear modulus, according to the relation $G=E/(2(1+v))$.

Therefore, a chiral structure tends to avoid localized deformation and the application of a load obtains an overall variation of shape at moderate local strain levels. Such property has been exploited in several studies that have assessed the possibility to design or manufacture an airfoil with a chiral honeycomb core for morphing purposes, such as in Bornengo *et al.* (2005), Spadoni and Ruzzene (2007), Martin *et al.* (2008). However, manufacturing of chiral cores involves several difficulties. Many of the experimental studies on chiral structures are performed by producing plastic elements by means of rapid prototyping, though metallic solutions, machined from a bulk plate, have been considered. The availability of a technology for the production of composite chiral cores, developed in Bettini *et al.* (2010) and further refined in Airoldi *et al.* (2011) makes possible manufacturing of chiral units with very thin, light and structurally effective ligaments, characterized by high strains to failure and an enhanced design flexibility, due to the possible choice of material and lay-ups. Composite chiral honeycombs have been specifically considered for the development of morphing concepts in Airoldi *et al.* (2012a) and Bettini *et al.* (2010). Such structural solutions based on composite chiral honeycomb are applied to passive morphing concepts and do not require the application of actuators.

2.2 Configuration and FE model of the aileron internal structure

In the present work, a chiral composite internal structure is considered for the development of an airfoil with a morphing trailing edge, which can be considered as an aileron with an internal morphing structure covered by a flexible skin. The chosen profile is shown in Fig. 2(a). It derives

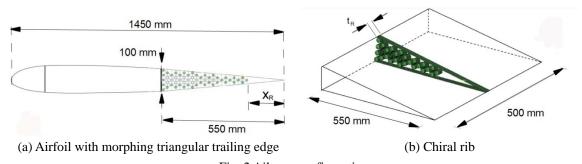(a) Airfoil with morphing triangular trailing edge　　　　　(b) Chiral rib

Fig. 2 Aileron configuration

from a NACA 65209 airfoil having a chord length of 1450 mm, with the morphing trailing edge represented by a 550 mm long and 100 mm thick triangular profile. In the morphing solution considered, the internal structure consists of chiral ribs, with a thickness t_R, shown in Fig. 2(b).

Each rib has the function to control the profile shape and to transmit the forces to the forward non-morphing wing structure under the action of the aerodynamic forces collected by the skin along a span length of 500 mm, as it shown in Fig. 2(b). The internal flexible cores of the ribs end at a distance x_R and the terminal of the rib will be considered rigid. Two different hexa-chiral topologies were selected to design the rib with identical ligament lengths, but different node radii. Such topologies will be referred to as coarse and dense chiral configuration, respectively. The parameter x_R, shown in Fig. 2(a) is also different for the two cases, because in the dense configuration the flexible core occupies a longer section of the aileron, before the terminal rigid end. The two types of rib also have different thickness, t_R. The main geometrical features are summarized in Table 1. In the chosen configuration, the ratio of the span length to the rib thickness greatly affects the stiffness and the strength required to the single rib to perform its functions. Indeed, the stiffness required to control the profile shape and to adequately transmit the aerodynamic loads could be obtained by adopting different configurations with different rib spacing. Since the in-plane stiffness of the chiral topology mainly depends on bending stiffness of the ligaments, the number of ribs could be, for instance, increased and the ligament thickness decreased in order to obtain the same overall stiffness of the internal structure of the airfoil. Alternatively, the rib thickness t_R could also be changed. By properly sizing the ribs, such different choices would lead to same stiffness and would not affect the morphing performance of the aileron, but it is worth noting that they would significantly influence the force and the stress acting in the chiral ligaments of the rib. For such reasons stress analyses will not be performed in this work, considering that the paper mainly investigates the aeroelastic performance of the morphing solutions and that the feasibility of morphing structures based on composite chiral cores was already completely addressed in Bettini *et al.* (2010) and Airoldi *et al.* (2012a). However, the previous considerations indicate that rib spacing could be a fundamental parameter to control

Table 1 Geometrical parameters of chiral honeycomb cores

		Coarse chiral	Dense chiral
L	(mm)	10	10
r/L	(-)	0.9	0.5
x_R	(mm)	214	136
t_R	(mm)	28.9	14.5

(a) Coarse configuration   (b) Dense configuration

Fig. 3 FE models of chiral ribs
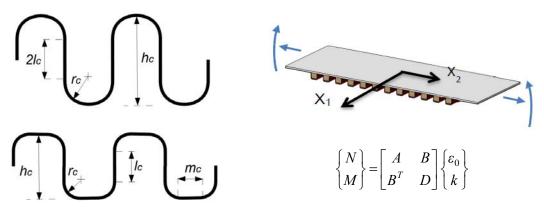
stress levels in the chiral topology.

For the development of the numerical approach, the finite element models of the two rib configurations were created and solved by using Abaqus/Standard (Abaqus (2010)). The numerical models, shown in Fig. 3, consist of about 9000 and 20000 elements for the coarse and refined topology, respectively. Linear shell (*S4* elements) and beam elements (*B31* elements) are used to model chiral ligaments and nodes, the skin and the beam connections. The forward and terminal ends are rigid bodies, which are connected to the first and last column of chiral nodes by means of kinematic links that make possible node rotation, in order to better exploit core flexibility and reduce the stress in the ligaments, as it was suggested in Bettini *et al.* (2010). The composite ligaments and nodes are represented by laminated shell with a uniform 0°-lay-up of fabric carbon/epoxy plies with the following in-plane stiffness properties: $E_{11} = E_{22} = 56650$ MPa, $G_{12} = 4043$ MPa, $v_{12} = 0.5$. Ply thickness is set to 0.1 mm. The model of the external skin and the connection with the chiral core are discussed in the following sub-section of the paper.

2.3 Technological solutions and model of the morphing skin

Realistic solutions for morphing structures have to take into account the need of a flexible external skin that must fulfill specific requirements. The functional role of the skin can be understood by considering that it must properly interact with the airstream in variable configurations. Indeed, the stiffness required to avoid excessive local deformation under the action of aerodynamic loads must not interfere with the capability of undergoing large and recoverable strains, in order to attain the required shape variations without failures, as it is discussed in Gandhi and Anusonti-Inthra (2008). A compromise can be found by developing skin systems that can be easily stretched in their plane but still present an adequate flexural stiffness to avoid local bubbling or buckling. Indeed, the skin should also present stiffness and load carrying capability in non-morphing directions, in order to reduce the need of additional structural elements in the morphing structure. In particular, for the aileron considered in this work, the stiffness in the span-wise direction plays a mean role for the transmission of aerodynamic loads to the ribs.

Corrugated composite laminates represent an interesting engineering solution for the fulfillment of the aforementioned requirements and were proposed by Yokozeki *et al.* (2006) for the production of highly anisotropic plates to be used in morphing structures. Two geometries for corrugated laminates are shown in Fig. 4(a). The stiffness in various directions and the maximum elongation can be significantly changed by varying the geometrical parameters of the corrugated geometry. A complete skin system can be obtained by coupling the composite corrugate with an elastomeric cover (Fig. 4(b)) in order to obtain a smooth external surface. A technological solution for such system is presented in Fournier *et al*. (2013).

The generalized laminate matrix, reported in Fig. 4(b), gives the possibility to efficiently represent the skin system in the FE models of the morphing structure, avoiding the need of modeling the detailed geometry of the corrugated laminate. A similar approach has been followed for the design of the passive system in Airoldi *et al.* (2005), where the skin was modeled by directly introducing the stiffness matrix of a symmetric laminate, with pre-defined properties in the span-wise direction. Membrane and bending stiffness in the chord-wise direction were obtained by means of an optimization process. The stiffness matrix adopted in such work can be considered an initial guess for the development of the aileron in the FE model. Considering the reference frame indicated in Fig. 4(b), the generalized stiffness matrix attributed to the skin is expressed as in the

$$\begin{Bmatrix} N \\ M \end{Bmatrix} = \begin{bmatrix} A & B \\ B^T & D \end{bmatrix} \begin{Bmatrix} \varepsilon_0 \\ k \end{Bmatrix}$$

(a) Corrugated laminates   (b) Complete skin and generalized stiffness matrix
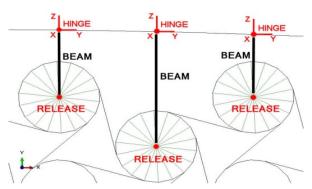
Fig. 4 Morphing skin concept

Fig. 5 Model of the skin-rib connection

following equation.

$$Q = \begin{bmatrix} A & B \\ B^T & D \end{bmatrix} = \begin{bmatrix} 60473 & 33.6 & 0 & 0 & 0 & 0 \\ 33.6 & 5.376 & 0 & 0 & 0 & 0 \\ 0 & 0 & 2608.1 & 0 & 0 & 0 \\ 0 & 0 & 0 & 140000 & 172.54 & 0 \\ 0 & 0 & 0 & 172.54 & 507.39 & 0 \\ 0 & 0 & 0 & 0 & 0 & 327.2 \end{bmatrix}$$

(1)

where membrane and flexural stiffness terms are given Nmm^{-1} and Nmm, respectively.

It is worth noting that the models presented in Fig. 3 do not represent the complete skin of the considered aileron section, presented in Fig. 2(b), but only the skin strip in correspondence of the rib, having the widths t_R, listed in Table 1. To reduce the size of the FE model, the complete skin was not modelled, but the stiffness terms in Eq. 1 in the span direction, A_{22} and D_{22}, were corrected by a factor equal to the ratio of span length to rib thickness, so to represent the stiffness of a skin panel having a width of $b = 500$ mm in the span-wise direction, as shown in Fig. 2(b).

In correspondence with the rib, the corrugated laminate is considered connected to the nodes of the chiral structure through a system of beam hinged at the ends. Considering an idealization of the skin as an anisotropic plate, the connection can be modeled by using beam elements that are set between the center of the chiral nodes and the FE nodes of the skins. Such modeling technique is illustrated in Fig. 5. Metallic or polimeric lugs and bushes can bonded and inserted in the corrugated laminates and in the nodes of the chiral core to physically realize the connection sketched in the figure.
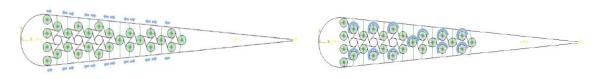
2.4 Actuation system

The skin and the connection with the chiral ribs are considered as potential locations for the installation of actuation systems.

Indeed, the skin system consisting of a composite corrugated panel covered by an external elastomeric skin is well-suited for the application of diffused actuation systems. In particular, wires of shape memory alloys (SMA) or skins made of shape memory polymers (SMP) could be embedded in the system and used to obtain a contraction of the skin. The two types of actuators are compared in Leng *et al.* (2011). Both SMA and SMP systems can be activated by heating and contract in order to recover an original shape. During activation typical Nichel-Titanium SMA can exert actuation stress of approximately 100 MPa and can recover strains up to 8%. SMP have significantly lower actuation stress (approximately 2 MPa – 10 MPa) but may recover very large strains, up to 400%.

Moreover, one-way SMA actuators can be arranged in a so-called antagonistic configuration, such as the one described in Sofla *et al.* (2008), so that the heated contracting skin can elongate the skin on the opposite side of the airfoil. Indeed, the detailed definition of the actuation system is beyond the scope of this work, which is mainly aimed at exploring the potential of the actuation solutions. Therefore, the action of the actuators is idealized by dividing the skin into several sections, which can be elongated or compressed by a system of forces acting in the skin plane, as it shown in Fig. 6(a).

A different strategy for the actuation of the morphing aileron is based on the application of a relative displacement between the skin and chiral rib. The connection between the nodes of the chiral rib and the corrugated skin, sketched in Fig. 4, is suited for the application of electric micromotors or, alternatively, piezo rotating motors or rotative actuators based on shape memory alloy. Different types of electric micromotors, such brushed, brushless or stepped motors, can apply moments as high as 600 Nmm, if endowed with a reduction gearbox, with a total weight of the order of one hundred of grams. The idealization of such actuation system in the FE model of the actuator is represented in Fig. 6(b). The effect of the actuation is represented by a system of

(a) SMA or SMP actuated skin   (b) Actuation system at skin/rib connections

Fig. 6 Models of actuation concepts

(a) SMA or SMP actuated skin   (b) Actuation system at skin/rib connections
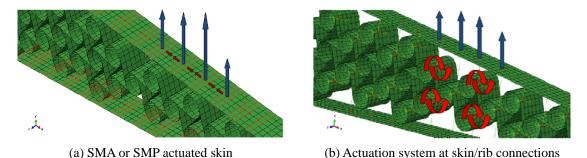
Fig. 7 Force systems applied in the FE model of the aileron

opposite moments, which are applied to the center of selected chiral nodes and to the rods that connect the chiral structure to the shell element of the skin, as shown in Fig. 4.

3. Aeroelastic condensed model of the actuated aileron

3.1 Condensation of the structural model

Considering the two chiral configurations, presented in Fig. 3, and the two actuation concepts, represented in Fig. 6, four type of aeroelastic models of the actuated aileron were developed. The numerical approach chosen is based on a reduced condensed model of the aileron structure, which was obtained by applying a Guyan condensation technique to the whole model that retained only the degrees of freedom (d.o.f.) where external aerodynamic forces acting on the aileron, F_{Aa}, and internal actuation forces, F_{act}, are applied.

The force systems applied for the two actuation concepts are represented in Fig. 7. The vertical arrows represent the aerodynamic forces that are applied to a set of discrete nodes according to the aerodynamic model that is presented in the Section 3.2. In the solution based on the actuated skin, actuation was represented by pairs of opposite forces, F_{act} and - F_{act}, acting at the ends of each skin segments between the beams connecting the skin to the chiral nodes (Fig. 7(a)). Only the vertical components of aerodynamic forces and the horizontal components of the actuation forces were considered in the model. In the solution with the actuation system set at the skin/rib connection, a couple of opposite moments, which are again denoted as F_{act} and - F_{act}, were applied to two rotational degrees of freedom that are superimposed at the centers of the chiral nodes: the first degree of freedom represents the rotation of the rigid body connected to the chiral node, whereas the second one is the rotational degree of freedom of the connection beam between the chiral structure and the skin (Fig. 7(b)).

The degrees of freedom of the finite element model were divided into a set of internal d.o.f.'s, u_i, and a set of external structural d.o.f.'s, u_S, where forces are applied. The stiffness matrix of the model was partitioned and a condensed matrix $[K_S]$ was defined

$$\begin{bmatrix} K_{cc} & K_{ci} \\ K_{ic} & K_{ii} \end{bmatrix} \begin{Bmatrix} u_S \\ u_i \end{Bmatrix} = \begin{Bmatrix} F \\ 0 \end{Bmatrix} \tag{2}$$

$$\left[K_{cc} - K_{ci}K_{ii}^{-1}K_{ic}\right]\{u_S\} = \{F\} \quad \Rightarrow \quad [K_S]\{u_S\} = \{F\}$$

Operatively, the condensed stiffness matrix of the four FE element models was calculated by using an Abaqus/Standard sub-structuring procedure, described in Abaqus (2010).

3.2 Aerodynamic model

The airstream around the airfoil was considered incompressible and inviscid and modeled by using a steady two-dimensional discrete vortex method. Following the approach described in Katz and Plotkin (1991, Chapter 11), the mid-line of the airfoil, including both the rigid part and the morphing aileron, was divided into N panels, as it is represented in Fig. 8. For each panel a lumped vortex element, with an unknown circulation Γ_i, is added to represent the integral of the local vorticity distribution. These vortices induce a potential velocity field and the Γ_i circulations can be evaluated by imposing the zero normal flow boundary conditions on the airfoil surface, which depend on the orientation of the panels, described by normals $\mathbf{n}_i$. The method leads to the following linear system for the computation of circulations (Eq. (3)).

$$[AIC]\{\Gamma\} = \{-U_\infty \cdot \mathbf{n}\} \tag{3}$$

where the matrix $[AIC]$ is the matrix of aerodynamic influence coefficients, that are necessary to compute the normal velocity due to the discrete vortices, and U_∞ is the free-stream velocity.

A simplification was introduced by considering that panel orientation depends only on the vertical displacement u_A of the nodes of the aerodynamic model, set along the mid-line of the whole profile. A geometrical matrix $[D]$ was defined to obtain the circulations as a function of vertical displacements, as in Eq. (4)

$$\{\Gamma\} = -U_\infty[AIC]^{-1}[D]\{u_A\} \tag{4}$$

Once that the expression of the circulations is developed, the forces acting on each node of the aerodynamic model, are obtained by using the Kutta-Joukowski theorem. A projection matrix $[J]$ is required, which takes the uniform pressure resultant acting on each panel and projects it on the
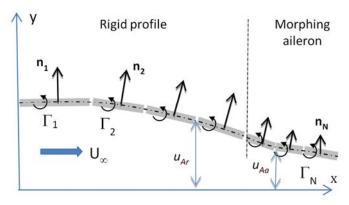

Fig. 8 Panel discrete vortex method applied to model aerodynamic forces

aerodynamic nodes. The vector of aerodynamic forces reads

$$\{F_A\} = -\rho U_\infty^2 [J][AIC]^{-1}[D]\{u_A\} = [K_A]\{u_A\} \tag{5}$$

where matrix $[K_A]$ represents the aerodynamic stiffness term.

The vector obtained in Eq. (5) includes both the forces acting on the rigid profile, F_{Ar}, and on the morphing aileron, F_{Aa}. Since the aeroelastic model is referred only to the aileron, the aerodynamic stiffness matrix was partitioned and the aerodynamic forces acting on the aileron were expressed as the sum of a term depending on the position of the mid-line in the rigid forward part of the profile and a term depending on the displacement of the mid-line in the morphing aileron. Moreover, since the profile was considered at a constant angle of attack in all the calculation, the forces depending on the position of the forward part were considered fixed

$$\{F_A\} = \begin{Bmatrix} F_{Ar} \\ F_{Aa} \end{Bmatrix} = \begin{bmatrix} K_{Arr} & K_{Ara} \\ K_{Aar} & K_{Aaa} \end{bmatrix} \begin{Bmatrix} u_{Ar} \\ u_{Aa} \end{Bmatrix}$$

$$\{F_{Aa}\} = [K_{Aar}]\{u_{Ar}\} + [K_{Aaa}]\{u_{Aa}\} = \{F_0\} + [K_{Aaa}]\{u_{Aa}\} \tag{6}$$

The portion of loads that depends on the force vector $\{u_{Ar}\}$ has been denominated $\{F_0\}$, since it is independent from the shape variation of the morphing aileron.

3.3 Aeroelastic model

The correct evaluation of the morphing aileron performance requires the investigation of the static aeroelastic effects due to the interaction of the aerodynamic loads with the flexibility of the airfoil structure. In fact, the final shape assumed by the morphing aileron is due to a combination of the actuators loads and aerodynamic loads applied to the structure.

As a consequence, this evaluation requires the development of a coupled model that combines the reduced structural model of Eq. (2) with the aerodynamic loads of Eq. (6). However, the nodes of the aerodynamic panel discretization are not coincident with the nodes of the structural model; while the first belong to the airfoil mid-line, the second set of nodes is placed on the external surface of the aileron. An interface operator was needed considering that the position and the displacement of a node laying on the mid-line can be expressed as the average of the displacement of two nodes placed at the corresponding chord stations on the upper and the lower surfaces. Hence, the displacements u_{Aa} were expressed as a linear function of the displacement u_{Sa}, which are the vertical displacements of the skin nodes where aerodynamic forces are applied, as shown in Fig. 7. A rectangular interface matrix $[H_{AS}]$ was defined and the aerodynamic forces were expressed as a function of a subset of the structural d.o.f.'s

$$\{u_{Aa}\} = [H_{AS}]\{u_{Sa}\}$$

$$\{F_{Aa}\} = \{F_0\} + [K_{Aaa}][H_{AS}]\{u_{Sa}\} \tag{7}$$

The d.o.f's of the structural model were divided into subsets representing: (a) the d.o.f.'s where aerodynamic forces are applied u_{Sa}, and (b) the d.o.f.'s corresponding to the action of the couple of

opposite actuation forces for both actuation concepts. Each couple of forces or moments represents an actuator with a given force level $F_{att.}$ Indeed such actuation force acts on two d.o.f.'s and therefore nodes where actuation forces are applied were conveniently divided into two vectors, which are denoted u^+_{Satt} and u^-_{Satt}, and represent respectively, the sets of d.o.f's where positive and negative $F_{att.}$ are applied to. The aeroelastic model was assembled by applying the principle of virtual work, which reads

$$\{\delta u_S\}^T[K_S]\{u_S\} = \{\delta u_{Sa}\}^T[H_{Sa}]^T[K_{Aaa}][H_{Sa}]\{u_{Sa}\} + \{\delta u_{Sa}\}^T[H_{Sa}]^T\{F_0\} +$$
$$+ \{\delta u^+_{Satt}\}^T\{F_{att}\} + \{\delta u^-_{Satt}\}^T\{-F_{att}\}$$

(8)

where

$$\{u_S\}^T = \{u_{Sa} \quad u^+_{Satt} \quad u^-_{Satt}\}^T$$

(9)

Finally, by rearranging the terms and dropping the virtual displacement, the following linear system, representing the whole condensed model, was obtained

$$[K_S]\begin{Bmatrix} u_{Sa} \\ u^+_{Satt} \\ u^-_{Satt} \end{Bmatrix} - \begin{bmatrix} [H_{Sa}]^T[K_{Aaa}][H_{Sa}] & 0 & 0 \\ 0 & 0 & 0 \\ 0 & 0 & 0 \end{bmatrix}\begin{Bmatrix} u_{Sa} \\ u^+_{Satt} \\ u^-_{Satt} \end{Bmatrix} = \begin{Bmatrix} [H_{Sa}]^T\{F_0\} \\ F_{att} \\ -F_{att} \end{Bmatrix}$$

(10)

4. Application of the aeroelastic model

4.1 Performance indices of the morphing aileron

The aeroelastic model obtained in the previous section can be directly applied to calculate the deformed shape of the aileron under the action of the actuation forces in a given aerodynamic condition. The aerodynamic model can be applied to recovery the aerodynamic forces for the evaluation of the variation of lift coefficient, ΔC_L. The work performed by the actuation system is spent to move the aileron against the aerodynamic forces and to elastically deform the structure. From an energetic standpoint, the energy spent for the deformation of the internal structure is an additional cost that does not exist in the case of a rigid aileron and directly affect the requirements to the actuation system in terms of forces and energy. Accordingly, one of the main objective in the design of a morphing system should be considered the minimization of the energy required to obtain a certain lift. An index is required to quantify the energetic cost of actuation and to compare it with the case of a rigid aileron.

In a rigid aileron, it can be observed that, under the assumption of small deflections, both the lift increase, ΔL, and the hinge moment, C, linearly depend on the aileron deflection, δ. Therefore, the ratio between the lift increase and the hinge moment can be considered a constant. Moreover, both numerator and denominator can be multiplied by δ, thus leading to Eq. (11)

$$\Delta L/C = \delta\Delta L/(C\delta) = const$$

(11)

The denominator in Eq. (11) is an approximation of the work spent for the actuation of the

aileron, W_{act}. The deflection can be expressed as a function of the obtained lift, by introducing the dynamic pressure, q, the surface S and the derivative $c_{l/\delta}$

$$\delta = \frac{\Delta L}{qSc_{l/\delta}} = \frac{\Delta L}{K(q)} \tag{12}$$

Accordingly, the previous ratio between lift and hinge moment can be expressed as

$$\frac{\Delta L}{C\delta}\delta = \frac{\Delta L}{C\delta}\frac{\Delta L}{K(q)} = \frac{\Delta L^2}{W_{act}}\frac{1}{K(q)} = const \tag{13}$$

Eq. (13) indicates that, for a given dynamic pressure, the ratio between the square of the lift variation and the work performed to deflect the aileron is constant. Such ratio can be used to define an energetic performance index that can be evaluated both for the rigid aileron and the morphing one, where actuation work can be computed by summing up the contribution of the elements in the actuation system. For the morphing aileron the expression of the index is given in Eq. (14), where generalized actuation forces and relative displacements have different definitions for the case of actuation embedded in the skin and the actuation between the skin and chiral rib.

$$I = \frac{\Delta L^2}{W_{act}} = \frac{\Delta L^2}{\sum_i F_{att\,i}\Delta u_{att_i}} \tag{14}$$

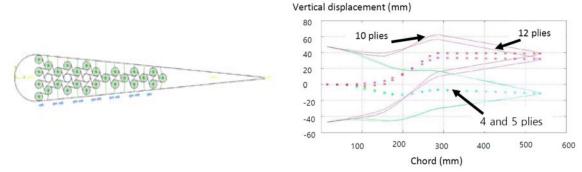### 4.2 Sensitivity studies presentation of selected configurations obtained

Four condensed aeroelastic models were developed to represent the solutions based on the coarse and the refined chiral structure with actuated skin and actuated skin/rib connections. A sensitivity study was performed by varying the thickness of the chiral ligaments in the range 0.4 mm ÷ 1.2 mm, forces in the actuated skin in the range 150 N ÷ 600 N and moment in the skin/rib connection in the range 150 Nmm ÷ 500 Nmm. The actuation systems were simplified by applying compressive forces only the lower surfaces and by considering rotary actuators applied only to a selected number of chiral nodes. Three velocity conditions were considered, namely 50 ms^{-1}, 100 ms^{-1} and 200 ms^{-1}. For such conditions, the value of the energetic performance indices referred to a rigid aileron were calculated and reported in Table 2. After preliminary results, the flexural stiffness attributed to the skin was increased at increasing velocity, in order to take into account the increment of dynamic pressure and to avoid the occurrence of skin bubbling.

The sensitivity study pointed out that the performances of the morphing aileron are greatly affected by the chosen combination of structural stiffness, actuation force and velocity. Some configurations showed very interesting results and are hereby discussed.

The first case presented is referred to a velocity of 100 ms^{-1}, a uniform actuation force of 300 N along the lower skin and a coarse chiral structure with different lay-ups made of 0° oriented plies

Table 2 Energetic index for a rigid aileron at three velocity conditions

U_∞	(ms[-1])	50	100	200
I	(Nmm[-1])	33.8	135.2	540.9

(a) Structural configuration   (b) Deformed shape for different lay-ups

Fig. 9 Configuration with coarse chiral structure, lower skin actuated with 300 N forces at 100 ms^{-1}

Table 3 Performance for a configuration with coarse chiral structure and actuated skin

		Ligament lay-up			
		4 plies	5 plies	10 plies	12 plies
ΔC_L	(-)	0.061	0.048	-0.390	-0.241
I	(Nmm^{-1})	21.60	14.40	-516	-362

(a) Structural configuration   (b) Deformed shape at different velocity
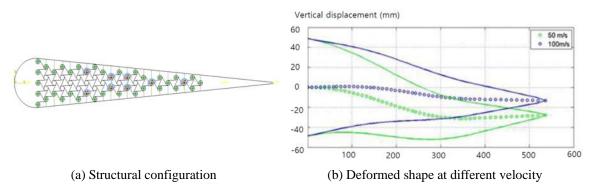
Fig. 10 Configuration with a 5-ply refined chiral structure and actuation moment of 500 Nmm

Table 4 Performance for a configuration with a 5-ply refined chiral structure and actuated skin/rib connection

		Velocity (ms^{-1})	
		50	100
ΔC_L	(-)	0.110	0.137
I	(Nmm^{-1})	11.2	155.0

having thickness of 0.1 mm. The structure and the shape obtained by actuating the skin are presented Fig. 9, whereas Table 3 reports the values of ΔC_L and energetic index for the same cases.

It can be observed that the system of actuation forces tends to bend the aileron towards in the downward direction, but such deformation is actually achieved only for low ligament thickness,

for instance when ligaments consists of 4/5 plies. The values reported in Table 3 indicate that a small variation of lift is obtained in such cases and that the energetic index is well below the one referred to the rigid aileron. When the stiffness of the chiral structure is increased an elastic hinge appears towards the rear end of the chiral honeycomb, where the structural configuration is more compliant. Toward the rear, the end of the aileron is translated in upward direction with a moderate rotation. Such configuration obtains significant negative values of ΔC_L are obtained. Moreover, the performance indices becomes higher than the corresponding value for the rigid case.

A second case is presented considering a refined chiral structure with actuation sets at the rib/skin connection. In particular, 8 moments with a value of 500 Nmm are applied to a set of selected chiral nodes, as it is shown in Fig. 10(a). The results reported in Fig. 10(b) are referred to the deformation obtained at 50 ms^{-1} and 100 ms^{-1} for a configuration with ligaments consisting of 5 plies. The variation of the lift coefficient and the energetic index reported in Table 4 are referred to the same structure and conditions.

In the cases presented in Fig. 10 and Table 4, the moments are applied to produce a rotation in the upward direction. However, the selected cases exploit the action aerodynamic forces in order to move the aileron in the downward direction and to produce a positive lift. Indeed, the deformation mechanism is similar to the one discussed in the comments to the solutions with the actuated skin. The local curvature is directed in the upward direction only in the rear part of the chiral structure, where local stiffness is low. The interaction with the aerodynamic forces produces a double curvature configuration and the end of the aileron tends to be aligned with the asymptotic velocity. For the case presented, the increment of lift coefficient is in the range 0.10÷0.15. The energetic indices at 50 ms^{-1} are about half of the ones referred to the rigid aileron, whereas at 100 ms^{-1} indices are similar to the ones of the rigid case.

Although several phenomena are not modelled in the simplified condensed model, the approach is adequate to capture the most significant aspects of the complex relations between stiffness, actuation forces and interaction with the air flow. Moreover, the most significant results obtained in the sensitivity study indicate that the force level applied to the actuation system can be varied to reach a condition that minimize the energy spent for an increment of the aerodynamic forces. Indeed, the selected cases previously presented are characterized by configurations where the local aerodynamic forces significantly contribute to the deformation of the aileron and to change the mid-line camber, thus generating on overall lift variation at a reduced energy cost.

However, it should be remarked that many of the combinations considered in the sensitivity study lead to very low levels of ΔC_L and of energetic index and that, in several cases, the idealized morphing system attains configurations characterized by excessive waviness of the aileron mid-line, with a several change of curvatures. The analysis of the available results indicates that the two phenomena, poor performances and excessive waviness of the configurations, could be correlated. Moreover, results also point out that certain combinations of velocity and stiffness correspond to a condition of static aeroelastic divergence. In such conditions, a minimal perturbation induced by the actuation system results in very large change of curvature and displacements.

4.3 Configurations identifed by optimization procedures

The sensitivity study pointed out the potential performances of the morphing solution. Interesting results were obtained although the number of design variables was limited, since the
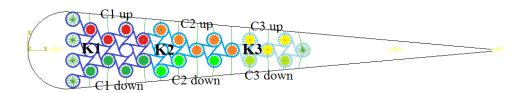
Fig. 11 Regions with different lay-up and actuation forces for the optimization process

stiffness of the internal chiral core and the actuation force levels were kept uniform along the aileron. It is reasonable to expect an improvement of the performance by adopting more design variables and by applying an optimization procedure to maximize performance indices.

Hence, a new parameterized model was created by identifying three separate regions for the chiral rib and the elements of the actuation system on the upper and lower skin. Each region was characterized by using different properties. The regions are indicated in Fig. 11, which is referred to a coarse chiral structure with skin/rib actuation. Regions K_1, K_2 and K_3 in the chiral structure are characterized by different ligament thickness. Actuation forces are differentiated by using six design variables that represent the force levels applied in six actuation regions, three acting on the upper skin and three on the lower skin of the aileron. The six design variables are denoted as $C_{i\text{-up}}$ and $C_{i\text{-down}}$ and the actuation regions are presented in Fig. 11.

An additional degree of freedom has been considered by varying the flexural stiffness of the skin. A lower bound, $D_{22\text{-min}}$, has been analytically identified by limiting the maximum deflection of the skin in the space interval between two adjacent supports under the action of a constant pressure. The skin flexural stiffness was allowed to vary between such lower bound and an upper bound set to $3 \cdot D_{22\text{-min}}$. The distance between two adjacent supports is different for the coarse and the refined chiral structure; therefore, the variation interval for the skin flexural stiffness is different for the two chiral topologies considered. By applying the analytical formulations presented in Yokozeki *et al.* (2006) and the material properties presented in Section 2.2, two sets of geometrical parameters of a corrugated laminate with flexural stiffness $D_{22\text{-min}}$ and $3 \cdot D_{22\text{-min}}$ were identified. Such parameters do not represent a unique possible combination, but are used to calculate reasonable values to bound the membrane stiffness A_{22} of the skin between a lower limit corresponding to $D_{22\text{-min}}$ and an upper limit corresponding to $3 \cdot D_{22\text{-min}}$. These bounds make possible to consider the membrane stiffness A_{22} as a dependent variable, proportional to D_{22}, which linearly varies between $A_{22}(D_{22\text{-min}})$ and $A_{22}(3 \cdot D_{22\text{-min}})$. The rationale behind this procedure is the adoption of realistic values for the skin stiffness by using a single design variable that represents a generalized stiffness property and does not involve the introduction of the detailed geometrical parameters. The followed approach guarantees that the values of membrane stiffness are consistent with the levels of flexural stiffness, which can be varied in a range where skin bubbling in operative conditions is avoided.

The optimization procedure was set up to maximize the energy performance index, with constraints regarding the maximum displacements and the eigenvalues of the complete stiffness matrix of the aeroelastic model. In particular, the minimum value of the real parts of all the eigenvalues was imposed to be higher than a given threshold, which actually depends on the level

of the structural stiffness, in order to avoid the occurrence of aeroelastic divergence. The formulation of the optimization procedure is summarized in Eq. (15).

$$\min\left(1\bigg/\left(\frac{\Delta L^2}{\sum\limits_i F_{att_i}\Delta u_{att_i}}\right)\right) \quad ; \quad \max(u_S)<50\,mm \quad ; \quad Min(\mathrm{Re}(\lambda_{aeroelastci}))>Threshold \qquad (15)$$

The formulation of optimization procedure was based on the assumption that configurations maximizing the energetic index and that are also far from aeroelastic divergence conditions should also present interesting value of ΔC_L. Moreover, on the basis of the sensitivity study, configurations with excessive waviness should be avoided by the procedure, since they should lead to poor performance indices. Actually, such assumptions did not resulted completely valid, in particular regarding the waviness of the mid-line for the morphing systems with actuated skin. In such a case, optimized configurations with several changes of curvature were obtained. Such tendency indicate that more complex optimization procedure are required to take into account the structural strength and the risk of flow separation due to excessive curvature of the profile.

On the contrary, the application of the optimization process to solutions with actuation set at the skin/rib connection provided quite interesting results, which confirm the tendencies outlined in sensitivity study and are characterized by noticeably improved performance indices. The presented results were obtained by considering a total number of 10 design variables, including structural and actuation parameters. In the optimization process a variation interval of -1500 Nmm ÷ +1500 Nmm was considered for all the six actuation moment levels $C_{i\text{-up}}$ and $C_{i\text{-down}}$, with $i = 1, 2, 3$. The number of plies K_1, K_2 and K_3 in the three regions of the chiral rib were varied between 3 and 16 plies. Finally, flexural stiffness for the coarse and refined chiral ribs were bounded in the intervals 422 Nmm ÷ 1267 Nmm and 213 Nmm ÷ 638 Nmm, respectively.

Optimization was performed by using the Ichrome/Nexus software (I-Chrome (2011)). The procedure was based on the reconstruction of meta-models, which were defined by applying an interpolation based on Kriging functions to the results of a Design of Experiments (DOE) performed in the variability domain of all the design variables. DOE points were evaluated by using Latin HyperCube allocation. Both the response surfaces of the cost function and of the constraints, expressed in Eq. (15), were evaluated for a set of about 3000 points in the domain
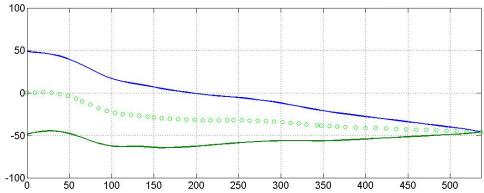

Fig. 12 Deformed configuration of the optimal solution with refined chiral rib and actuation at skin/rib connection

Table 5 Optimal solution with the refined chiral structure and actuated skin/rib connection

Upper actuation moments (Nmm)			Lower actuation moments (Nmm)		
$C_{1\text{-up}}$	$C_{2\text{-up}}$	$C_{3\text{-up}}$	$C_{1\text{-down}}$	$C_{2\text{-down}}$	$C_{3\text{-down}}$
191.9	-1158.9	-52	1087.6	138.9	426.5
Number of plies in ligaments			Skin flexural stiffness (Nmm)		
K_1	K_2	K_3		498.21	
4	12	12			

Table 6 Performance of the optimal solution with refined chiral structure and actuated skin/rib connection

I	(Nmm^{-1})	974.2
ΔC_L	(-)	0.446
$\text{Max}(u_s)$	(mm)	-45 mm

defined by the variability range of design variables. Meta-models were then used to carry out a constrained minimization process by applying a single-objective genetic algorithm.

Actually, the procedure was carried out in two subsequent steps. The first one considered a DOE in the previously defined variability domain for the 10 design variables. Such preliminary process lead to the identification of the most promising region in the domain of the design variables, and a subsequent DOE was performed in a restricted domain in order to obtain a reliable optimal configuration. Meta-models were obtained in the restricted domain and the genetic optimization algorithm was used to find the optimal configuration. Finally, the optimal set of parameters was verified by directly applying the aeroelastic model.

Table 5 presents the design parameter of the optimal solution identified for refined chiral structure, whereas Table 6 summarizes the performance indices. The deformed configuration is shown in Fig. 12.

The present solution obtain remarkable values of energetic index and lift coefficient increment. It can be observed that the optimization process lead to reduce the stiffness in the initial part of the morphing aileron, so to promote the development of an elastic hinge. In such a region, the curvature of the mid-line could probably be too large, on the basis of aerodynamic and structural considerations. However, the solution confirms that the most promising values of performance indices can be found by obtaining a translation of the final part of the aileron. It should be observed that a further reduction of the stiffness in the forward region of the chiral structure was rejected in the optimization process due to a violation of the constraints regarding aeroelastic divergence.

The deformed configuration for the optimal solution with the coarse chiral topology is presented in Fig. 13 and confirms the general trends in the behavior of the morphing system. Differently from the optimal solution for the refined rib, the deformed mid-line does not present localized elastic hinges, though a change of curvature can be observed. The design parameters of the solution are reported in Table 7. The values of the actuation moments are symmetric on the upper and lower surface and the initial part of the aileron is significantly more compliant than the other sections. The moments in the compliant zone tend to rotate the aileron downward. Actuation
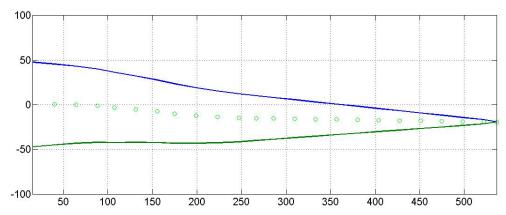
Fig. 13 Deformed configuration of the optimal solution with coarse chiral rib and actuation at skin/rib connection

Table 7 Optimal solution with coarse chiral structure and actuated skin/rib connection

Upper actuation moments (Nmm)			Lower actuation moments (Nmm)		
$C_{1\text{-up}}$	$C_{2\text{-up}}$	$C_{3\text{-up}}$	$C_{1\text{-down}}$	$C_{2\text{-down}}$	$C_{3\text{-down}}$
808.5	13.8	-1491.7	811.1	220	-1489.7
Number of plies in ligaments			Skin flexural stiffness (Nmm)		
K_1	K_2	K_3		951.4	
8	14	14			

Table 8 Performance of the optimal solution with coarse chiral structure and actuated skin/rib connection

I	(Nmm^{-1})	1336.7
ΔC_{L}	(-)	0.1804
$\text{Max}(u_s)$	(mm)	-19.5 mm

is almost removed in the central section whereas, in the rear part, moments are applied to rotate the aileron end in the counterclockwise direction and to align the rigid end in the direction of the airstream.

In Table 8, the performance indices are presented. The maximum of the energy index is very high, although it is attained in a configuration with a limited displacement and a moderate increment of lift.

5. Conclusions

The model of an actuated morphing aileron was developed by exploiting the properties of chiral topologies and applying actuation solutions based on different concepts. The numerical activity indicates that the response and the design flexibility of the composite chiral honeycomb play an important role in the performance of the morphing system. Indeed, the results confirm that a chiral rib can undergo significant displacements still maintaining the capability of sustaining and

transmitting the air loads applied to the skin. Moreover, the stiffness of the chiral core is a fundamental parameter to control the local shape of the airfoil and to obtain the progressive shape variations that characterize morphing solutions. The actuation strategies that were applied exploited the peculiar structural performance offered by the chiral core. The results obtained in the sensitivity study show that the a skin with a proper combination of membrane and flexural stiffness can be elongated and compressed by using a diffused actuation system and can be supported by a chiral core, which also control of the airfoil thickness and achieve a progressive shape variation. The results show also the potential of an actuation based on a discrete system of actuators, set at the connection between the inner structure and the external skin.

From the methodological standpoint, the work explored the potential of a computationally effective approach, based on a condensed aeroelastic model. Although the model is not accurate in the representation of the aerodynamic pressures, does not include any boundary layer and simplifies the response of actuators, such simplified approach highlights the importance of fluid-structure interactions in the design of morphing solution. Moreover, the definition of an energetic performance index made possible a quantification of the energetic cost involved in actuation.

It must be remarked that more refined models and optimization process are required to obtain feasible design solution that could satisfy all structural and aerodynamic requirements. However, the presented sensitivity study and the optimization processes identified the guidelines for the development of an actuation strategy that can maximize the beneficial effects of fluid structure interaction and reduce the requirements on the actuators in terms of forces and energy.

References

Abaqus (2010), *Analysis and User's Manual Version 6.10*, Dassault System.

Airoldi, A., Bettini, P., Zazzarini, M. and Scarpa, F. (2012a), "Failure and energy absorption of plastic and composite chiral honeycomb", *Structures Under Shock and Impact XII*, Schleyer, G. and Brebbia, C.A. (Ed.), WIT Press, Southampton.

Airoldi, A., Crespi, M., Quaranta, G. and Sala, G. (2012b), "Design of a morphing airfoil with composite chiral structure", *J. Aircraft*, **49**(4), 1008-1019.

Anderson, J.D. (1999), *A History of Aerodynamics and its Impact on Flying Machines*, Cambridge University Press, Cambridge, UK.

Baker, D. and Friswell, M.I. (2009), "Determinate structures for wing camber control", *Smart Mater. Struct.*, **18**(3), 035014.

Barbarino, S., Bilgen, O., Ajaj, R.M., Friswell, M.I. and Inman, J. (2011), "A review of morphing aircraft", *J. Intel. Mat. Syst. Str.*, **22**(9), 823-827.

Bettini, P., Airoldi, A., Sala, G., Di Landro, L., Ruzzene, M. and Spadoni, A. (2010), "Composite chiral structures for morphing airfoils: Numerical analyses and development of a manufacturing process", *Compos. Part B. Eng.*, **41**(2), 133-147.

Bornengo, D., Scarpa, F. and Remillat, C. (2005), "Evaluation of hexagonal chiral structure for morphing airfoil concept", *Proceedings of the Institution of Mechanical Engineers Part G, J. Aerospace Eng.*, **219**(3), 185-192.

Campanile, L.F. and Anders, S. (2005), "Aerodynamic and aeroelastic amplification in adaptive belt-rib airfoil", *Aerosp. Sci. Tech.*, **9**(1), 55-63.

Campanile, L.F. and Sachau, D. (2000), "The belt-rib concept: A structronic approach to variable camber", *J. Intel. Mat. Syst. Str.*, **11**(3), 215-224.

Gandhi, F. and Anusonti-Inthra, P. (2008), "Skin design studies for variable camber morphing airfoils", *Smart Mater. Str.*, **17**(1), 1-8.

Ichrome Ltd. (2011), *Nexus Documentation v. 1.1.07*.

Katz, J. and Plotkin, A. (1991), *Low-Speed Aerodynamics*, Cambridge University Press, Cambridge, UK.

Lakes, R.S. (1991), "Deformation mechanisms in negative Poisson's ratio materials: Structural aspects", *J. Mater. Sci.*, **26**(9), 2287-2292.

Leng, J., Lan, X., Liu, Y. and Du, S. (2001), "Shape-memory polymers and their composites: Stimulus methods and applications", *Prog. Mater. Sci.*, **56**(7), 1077-1135.

Martin, J., Heyder-Bruckner, J.J., Remillat, C., Scarpa, F., Potter, K. and Ruzzene, M. (2008), "The hexachiral prismatic wingbox concept", *Phys. Status Solidi. B.*, **245**(3), 570-577.

Sofla, A.Y.N., Elzey, D.M. and Wadley, H.N.G. (2008), "Two-way antagonistic shape actuation based on the one-way shape memory effect", *J. Intel. Mat. Syst. Str.*, **19**(9), 1017-1027.

Sofla, A.Y.N., Meguid, N.A., Tan, K.T. and Yeo, W.K. (2010), "Shape morphing of aircraft wing: Status and challenges", *Mater. Design*, **31**(3), 1284-1292.

Spadoni, A. and Ruzzene, M. (2007), "Numerical and experimental analysis of the static compliance of chiral truss-core airfoils", *J. Mech. Mater.*, **2**(5), 965-981.

Yokozeki, T., Takeda, S., Ogasawara, T. and Ishikawa, T. (2006), "Mechanical properties of corrugated composites for candidate materials of fexible wing structures", *Compos. Part A. Appl. S.*, **37**(10), 1578-1586.

EC